Active Polymers – Emergent Conformational and Dynamical Properties: A Brief Review

Roland G. Winkler, Jens Elgeti, and Gerhard Gompper^{a)}

Active matter exhibits a wealth of emerging nonequilibrium behaviours. A paradigmatic example is the interior of cells, where active components, such as the cytoskeleton, are responsible for its structural organization and the dynamics of the various components. Of particular interest are the properties of polymers and filaments. The intimate coupling of thermal and active noise, hydrodynamic interactions, and polymer conformations implies the emergence of novel structural and dynamical features. In this article, we review recent theoretical and simulation developments and results for the structural and dynamical properties of polymers exposed to activity. Two- and three-dimensional filaments are considered propelled by different mechanisms such as active Brownian particles or hydrodynamically-coupled force dipoles.

I. INTRODUCTION

Active matter, whose agents convert either internal chemical energy into directed motion, or utilize energy from the environment, 1,2 exhibit fascinating emergent dynamical and collective phenomena. Prototypes are omnipresent in nature and range from the macroscopic scale of flocks of birds, school of fish, and mammalian herds,³ over self-propelled algae, sperm, and bacteria on the single cell level^{1,4-6}, to the sub-cellular scale of the cytoskeleton in living cells. 3-5,7-14 The motion and collective behavior of active matter in the microworld is distinctively different from that of self-propelled bodies in the macroworld.^{1,2,4} This is due to at least four reasons: (i) Propulsion and motility in the microworld is typically governed by low-Reynolds number hydrodynamics, (ii) thermal and active noise plays an important role on length scales in the nano- and micrometer range, (iii) active agents are often highly deformable, and (iv) interactions in the microworld are of simple molecular origin. As a consequence, size, shape, and deformability of active particles is essential for their individual and collective behavior. The motion of active agents on the microscale is typically persistent and nearly deterministic, while that on the nanoscale is highly chaotic and nearly indistinguishable from random diffusive motion. Moreover, shape matters, spherical active Brownian particles (ABPs) lack any shape-induced alignment interaction when they collide, while rodlike Brownian particles align in parallel due to volume exclusion.

In this mini-review, we focus on the nonequilibrium behavior of active polymers and filaments. From a physical point of view, the most interesting aspect is the interplay of propulsion, deformability, and noise.

There are many realizations of active polymers. Enzymes which catalyze chemical reactions are active particles and shown enhanced translational diffusion¹⁵ and

chemotaxis. 16 In motility assays, biological semiflexible polar filaments, such as actin and microtubules, are propelled on carpets of motor proteins anchored on a substrate, which results in a directed motion. 11-14,17-19 Propulsion of such biological filaments in the cell cytoskeleton due to tread-milling and dimeric or tetrameric motor proteins is ubiquitous. Mixtures of active and passive components are a characteristics of eukaryotic cells with the active cytoskeleton on the one hand and an embedded large variety of passive colloidal and polymeric objects on the other hand. Here, an enhanced random motion of tracer particles has been observed.²⁰ Moreover, an influence of the active microtubule²¹ or actin-filament²² dynamics on the motion of chromosomal loci^{23,24} or that of chromatin has been found.²⁵ Active chains of metal-dielectric Janus colloids can be realized by a simultaneous control of colloid motility and interactions via a perpendicular a.c. electric field. ^{26,27} And. finally, chains of passive colloidal particles show nonequilibrium properties in an active environment.²⁸

Current studies of active filaments/polymers can crudely be classified into four categories. (i) Closest to individual active Brownian particles are polymers comprised of ABP monomers (cf. Fig. 1).^{29–38} Here, every monomer is independently changing its propulsion direction in a diffusive manner. A realization might be a passive polymer in a fluid of ABPs (cf. Fig. 1). In terms of a colored noise description of activity, their statistical properties are rather similar. 36,38. Explicitly, passive polymers in a bath of ABPs have been considered. 30,31,33,39 (ii) Motivated by the active dynamics of filaments in motility assays, ^{13,40} semiflexible polymers are considered which are propelled tangential to their contour. 41-45 Since the driving force has a preferred direction, such systems are denoted polar active polymers. (iii) Fluid mediated interactions are captured to a certain extent in models of either ABPs³⁵ or tangential propulsion^{46,47} with hydrodynamic interactions between the monomers due an induced fluid motion by monomer-monomer interactions. (iv) Most generally, the monomers produce spontaneous flow, which propel the whole polymer. 48,49 Such a approach corresponds to a force- and torque-free swimmer which, in principle, includes hydrodynamics. In this article, we discuss the various aspects of these ap-

a) Theoretical Soft Matter and Biophysics, Institute of Complex Systems and Institute for Advanced Simulation, Forschungszentrum Jülich, 52428 Jülich, Germany; Electronic mail: t.eisenstecken@fz-juelich.de, g.gompper@fz-juelich.de, r.winkler@fz-juelich.de

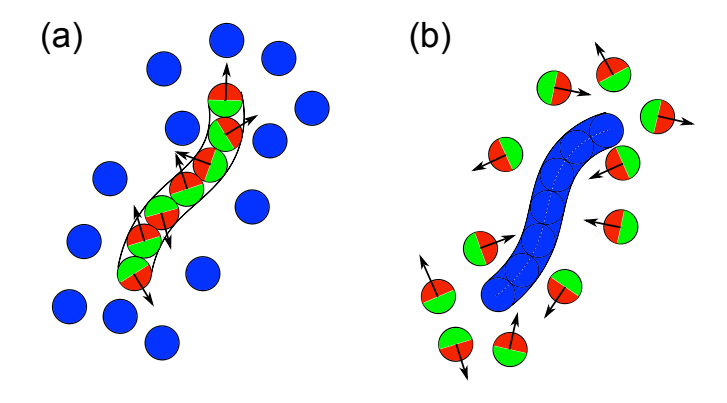


FIG. 1. (Color online) Illustration of a polymer exposed to active noise. (a) The polymer is comprised of active Brownian particles. (b) A passive polymer is embedded in a fluid with active Brownian particles.

proaches.

II. POLYMER EMBEDDED IN OR COMPRISED OF ACTIVE BROWNIAN PARTICLES

A. Active Brownian Particles

An active Brownian particles is a well established representation of a self-propelled object. $^{1,2,50-57}$ It is typically represented as a repulsive spherical colloidal particle propelled by a constant (external) force in the direction of its instantaneous orientation, which is changing in a diffusive manner. No hydrodynamic interactions are taken into account. The equations of motion for the center-of-mass position \boldsymbol{r} and the orientation \boldsymbol{e} are given by

$$\dot{\boldsymbol{r}}(t) = \boldsymbol{v}(t) + \frac{1}{\hat{\gamma}} \left(\boldsymbol{F}(t) + \boldsymbol{\Gamma}(t) \right), \tag{1}$$

$$\dot{\boldsymbol{e}}(t) = \hat{\boldsymbol{\eta}}(t) \times \boldsymbol{e}(t), \tag{2}$$

where $\mathbf{v} = v_0 \mathbf{e}$ is the propulsion velocity, \mathbf{F} a force exerted on the particle, $\mathbf{\Gamma}$ and $\hat{\boldsymbol{\eta}}$ are Gaussian and Markovian processes (white noise) with zero odd moments and the second moments

$$\langle \Gamma_{\alpha}(t)\Gamma_{\beta}(t')\rangle = 2\hat{\gamma}k_B T \delta_{\alpha\beta}\delta(t - t'), \tag{3}$$

$$\langle \hat{\eta}_{\alpha}(t)\hat{\eta}_{\beta}(t')\rangle = (d-1)D_R\delta_{\alpha\beta}\delta(t-t'). \tag{4}$$

Here, k_B is the Boltzmann constant, T the temperature, $\hat{\gamma}$ the translational friction coefficient, which is related to the translational diffusion coefficient D_T via $D_T = k_B T/\hat{\gamma}$, D_R the rotational diffusion coefficient, d is the spatial dimension, and $\alpha, \beta \in \{x, y, x\}$. For a particle in a viscous fluid in three dimensions (3d), $\hat{\gamma} = 6\pi\eta R$, with η the viscosity and R the particle radius, hence, D_R and D_T are related according to $D_T/D_R R^2 = 4/3$. The rotational motion (Eq. (2)) is independent of the colloid translation. As a particular result, the correlation

function

$$\langle \boldsymbol{v}(t) \cdot \boldsymbol{v}(t') \rangle = v_0^2 e^{-(d-1)D_R|t-t'|} \tag{5}$$

is obtained. $^{58-60}$

B. Theoretical Description of the Conformational and Dynamical Properties of Active Semiflexible Polymers

Analytically, the conformational and dynamical properties of active polymers have been studied by the Rouse model^{34,35,37}, for flexible polymers, or by extensions thereof for semiflexible polymers^{32,36,38}. Activity is taken into account as a random force with an exponential temporal correlation, *i.e.*, as colored noise (Eq. (5)).^{1,32,35,36,57} Here, activity can be interpreted in two ways. On the one hand, the polymer may be considered as comprised of active monomers, *e.g.*, active Brownian particles (ABPs). On the other hand, the active force can originate from interactions with uncorrelated surrounding ABPs, hence, the polymer corresponds to a passive polymer dissolved in an active bath (cf. Fig. 1).³⁶ Respective computer simulations are provided in Secs. II C and II D.

We briefly describe the main conformational and dynamical properties of polymers in presence of active noise utilizing a Gaussian semiflexible polymer model $^{58,61-63}$ The polymer of length L experiences an active random force $\mathbf{F}_a(s,t) = \gamma \mathbf{v}(s,t)$ at the position $\mathbf{r}(s,t)$ along its contour at s and time t, where γ is the translational friction coefficient per length and \mathbf{v} is a non-Markovian, but Gaussian stochastic process with zero odd moments and the second moment 36

$$\langle \boldsymbol{v}(s,t) \cdot \boldsymbol{v}(s',t') \rangle = v_0^2 l e^{-\gamma_R |t-t'|} \delta(s-s') .$$
 (6)

In a touching-bead model, the length l corresponds to the diameter of a bead. The decay of the correlation is determined by $\gamma_R = (d-1)D_R$, where D_R is the rotational diffusion coefficient of an ABP (cf. Sec. II A). In this section, we restrict ourselves to three dimensions. More details on the derivation of Eq. (6) are presented in Ref.³⁶. In addition, thermal fluctuations are captured by the Brownian white noise $\Gamma(s,t)$ (3). The overdamped linear equation of motion for the polymer can be solved analytically by a normal-mode analysis. Explicitly, the position $\mathbf{r}(s,t)$ is given by

$$\mathbf{r}(s,t) = \sum_{n=0}^{\infty} \mathbf{\chi}_n(t) \varphi_n(s)$$
 (7)

in terms of the eigenfunctions $\varphi_n(s)$ and the normal mode amplitudes $\chi_n(t)$. The latter become

$$\chi_n(t) = \int_{-\infty}^t e^{-(t-t')/\tau_n} \left(\boldsymbol{v}_n(t') + \frac{1}{\gamma} \boldsymbol{\Gamma}_n(t') \right) dt' \quad (8)$$

in the stationary state. Here, $v_n(t)$ and $\Gamma_n(t)$ are the normal mode amplitudes of the random active velocity and

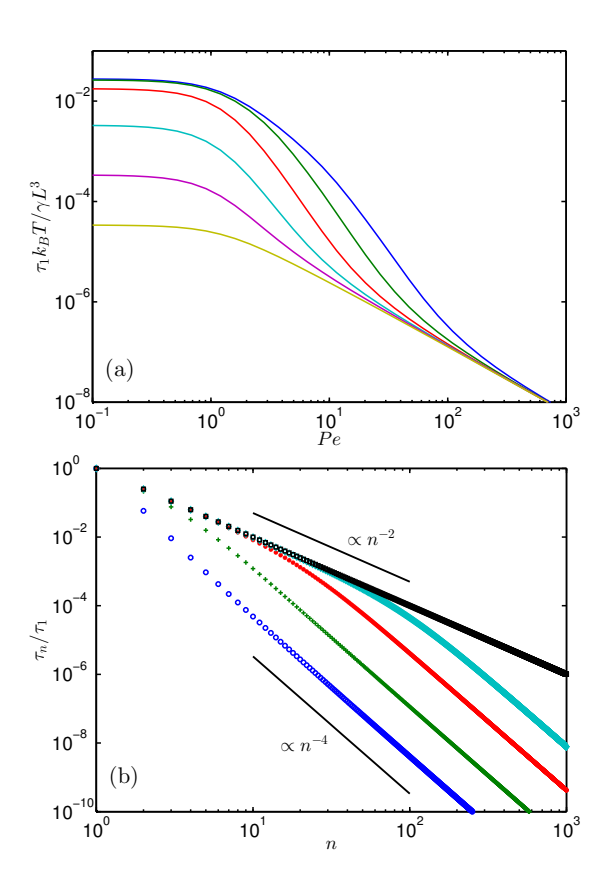


FIG. 2. (Color online) (a) Longest polymer relaxation times as function of the Péclet number for the bending stiffnesses (L is fixed) $L/2l_p=10^3$, 10^2 , 10, 1, 10^{-1} , and 10^{-2} (bottom to top). (b) Mode-number dependence of the relaxation times of active polymers with $L/2l_p=10^{-2}$ for the Péclet numbers $Pe=10^1$, 3×10^1 , 10^2 , and 5×10^2 (bottom to top). The black squares (top) show the mode-number dependence of a flexible polymer with $L/2l_p=10^3$. The solid lines indicate the relations for flexible ($\sim n^{-2}$) and semiflexible ($\sim (2n-1)^{-4}$) passive polymers, respectively. (From Ref. ³⁶)

the thermal noise, respectively. The eigenvalue equation yields the relaxation times (n>0)

$$\tau_n = \frac{\gamma}{k_B T(\epsilon \zeta_n^4 + 2\lambda \zeta_n^2)} \tag{9}$$

in terms of the activity-dependent wave numbers ζ_n , where the bending coefficient $\epsilon = 3l_p/2$ accounts for bending restrictions, l_p is the persistence length, and λ is the activity-dependent bond-stretching coefficient. The latter is determined in a mean-field manner by the constraint of a finite polymer contour length L.³⁶

1. Relaxation Times

The dependence of the longest relaxation time τ_1 on the Péclet number, defined as

$$Pe = \frac{v_0}{D_R l},\tag{10}$$

is illustrated in Fig. 2(a). Evidently, the relaxation times exhibit a strong dependence on Pe. In particular, they decrease with increasing Pe and approach a stiffness-independent asymptotic value for $Pe \to \infty$. Hence, activity accelerates the polymer relaxation behavior. For flexible polymers $(L/2l_p \gg 1)$, the relaxation times follow as 36,38

$$\tau_n = \frac{\tau_R}{\mu n^2},\tag{11}$$

with $\mu=4l_p\lambda/3$, the bond-stretching coefficient scaled with respect to the value of a passive flexible polymer, and $\tau_R=2\gamma l_p L^3/3\pi k_B T$ the Rouse relaxation time. ^{36,58,63} The coefficient μ captures the activity dependence of the relaxation times.

For $Pe\gg 1$ and a large number of active sites L/l, the calculations yield $\mu\sim Pe^{4/3}$ and for a small number L/l, $\mu\sim Pe$, which implies the dependencies $\tau_n\sim Pe^{-4/3}$ and $\tau_n\sim Pe^{-1}$ ($Pe\gg 1$), respectively. Activity exerts forces on the bonds, attempting to stretch them. The increase in the bond-stretching coefficient counteracts activity and maintains a (mean) constant contour length. Hence, the characteristics of a polymer, namely a fixed contour length, implies a specific response to active noise. Neglecting the factor μ , as in typical Rouse model description, 32,34,35,37,64 leads to significantly different relaxation times and neglects a substantial Péclet-number dependence of active system.

At $Pe\lesssim 1$, the relaxation times of stiff polymers are determined by the bending modes. With decreasing $L/2l_p$, τ_1 approaches the persistence-length and Pe-independent value $\tau_1=\gamma L^3/36k_BT$ (cf. Fig. 2(a)). With increasing Pe, the bond-stretching coefficient increases fast and, as a consequence, τ_1 decreases rapidly approaching asymptotically the relaxation time of a flexible polymer. The "softening" of semiflexible polymers is even more evident from the relaxation times τ_n of a stiff polymer displayed in Fig. 2(b). The passive polymers exhibit the well-known n^{-4} mode-number dependence. An increasing activity implies a gradual change toward n^{-2} , and ultimately, at $Pe\gg 1$, the mode-number dependence of a flexible polymer is obtained over a considerable range of mode numbers.

2. Conformations: Mean Square End-to-End Distance

The conformational properties of the polymers can be characterized by their mean square end-to-end distance $(\langle r_e^2 \rangle = \langle (r(L/2) - r(-L/2))^2 \rangle)$, which, in terms of the eigenfunction expansion, is given by

$$\langle r_e^2 \rangle = 4 \sum_{n=1}^{\infty} \left(\frac{3k_B T}{\gamma} \tau_{2n-1} + \frac{v_0^2 l}{1 + \gamma_R \tau_{2n-1}} \tau_{2n-1}^2 \right) \varphi_{2n-1}^2(L/2).$$
(12)

Results are shown in Fig. 3 for various persistence lengths. The dependence of the relaxation times on the

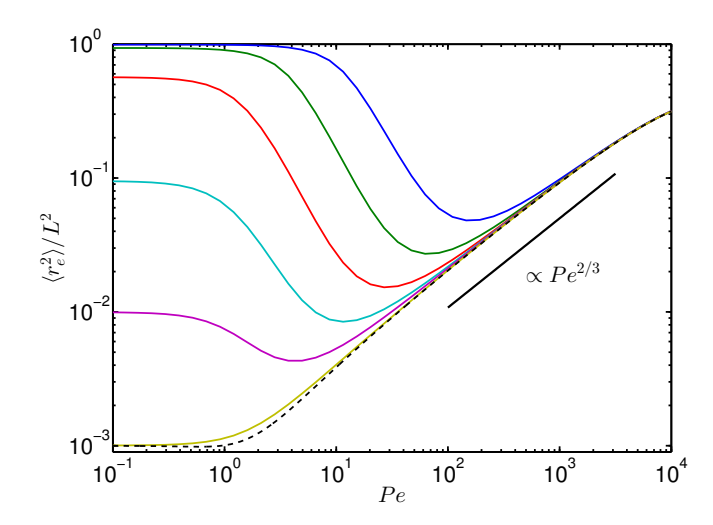


FIG. 3. (Color online) Mean square end-to-end distances according to Eq. (12) as function of the Péclet number for the ratios $L/2l_p=10^3$, 10^2 , 10, 1, 10^{-1} , and 10^{-2} (bottom to top at $Pe=10^{-1}$). The dashed line represents an approximate analytical solution. (From Ref.³⁶)

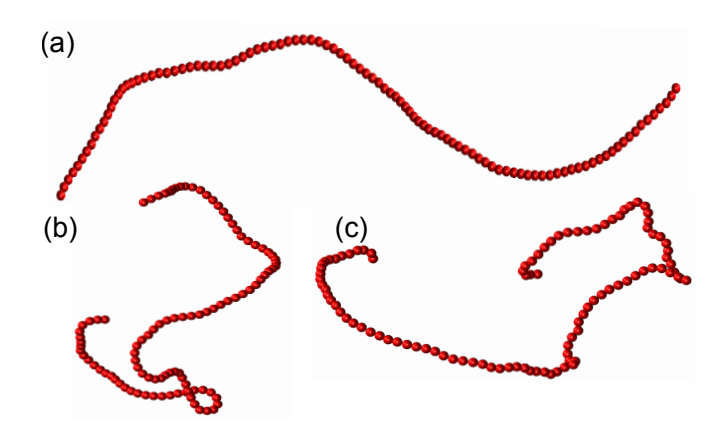


FIG. 4. (Color online) Snapshots of an active semiflexible polymer comprised of N=100 ABPs with $L/2l_p\approx 0.1$. (a) The polymer is semiflexible (Pe=1), (b) shrinks with increasing activity (Pe=20), and (c) swells again with further increasing Pe (Pe=100).

activity determines the polymer conformations. If the relaxation times were independent of the active noise, the active-noise contribution to $\langle r_e^2 \rangle$ would increase quadratically with v_0 , and hence, with the Péclet number. Here, we find the significantly slower increase of $\langle r_e^2 \rangle \sim Pe^{2/3}$ with increasing Pe. There are several remarkable features of $\langle r_e^2 \rangle$ for the various persistence lengths. For flexible polymers, $\langle r_e^2 \rangle$ increases monotonically in a sublinear manner in the range $1 \ll Pe < 10^3$ and approaches the asymptotic value $L^2/2$ in the limit $Pe \to \infty$ as a consequence of the finite contour length; interestingly, the polymers are not fully stretched in this limit. At large persistence lengths, $\langle r_e^2 \rangle$ shows a nonmonotonic

dependence on the Péclet number. Within a certain persistence-length-dependent range, a polymer shrinks with increasing Pe (cf. Fig. 4). The shrinkage can be substantially for $pL \lesssim 10$. Above a certain Pe value, the polymers swell again and approach the asymptotic dependence of a flexible polymer as a consequence of the dominating flexible modes in the relaxation times. It is important to note that the detailed quantitative activitydependent behavior is a function of the number L/l of active sites along the polymer. In a typical simulation, with a polymer comprised of ABP monomers³⁴, this corresponds to the number of monomers. We have performed computer simulations of a discrete polymer in three dimensions comprised of ABPs, which yield results in close agreement with the theoretical prediction. In particular, the shrinkage of semiflexible polymers and the general swelling are confirmed (Fig. 1).

3. Dynamics: End-to-End Vector Relaxation

The correlation function of the polymer end-to-end vector is given by³⁸

$$\langle \boldsymbol{r}_{e}(t) \cdot \boldsymbol{r}_{e}(0) \rangle = \sum_{n=1}^{\infty} \varphi_{2n-1} (L/2)^{2} \left[\frac{4L^{3}}{\hat{\xi}_{2n-1}} e^{-t/\tau_{2n-1}} + \frac{Pe^{2}l^{3}}{9\Delta^{2}\hat{\xi}_{2n-1}^{2}l^{6}/(4L^{6}) - 1} \left(e^{-\gamma_{R}t} - \frac{2L^{3}}{3\Delta l^{3}\hat{\xi}_{2n-1}} e^{-t/\tau_{2n-1}} \right) \right]$$

$$(13)$$

using the eigenfunction expansion (7), where $\hat{\xi}_n = L\mu(\zeta_nL)^2/2l_p + l_p(\zeta_nL)^4/2L$). Two relaxation mechanisms govern the decay of the correlation function, the rotational Brownian motion of an individual ABP $(\gamma_R t)$ and the dynamics of the polymer itself (t/τ_n) . In the limit $\gamma_R \tau_1 \gg 1$, which is equivalent to $Pe \ll (L/l)^{3/2}$, the decay of the correlation function is determined by the relaxation times of the polymer. For $t/\tau_1 > 1$, the decay is exponential

$$\langle \boldsymbol{r}_e(t) \cdot \boldsymbol{r}_e(0) \rangle = \frac{L^3}{\hat{\xi}_1} e^{-t/\tau_1} \left(4 + 2Pe^2 \right) \varphi_1(L/2)^2.$$

Since activity leads to shorter relaxation times, the decay is enhanced by the active noise. In the opposite limit $\gamma_R \tau_1 \ll 1$, the correlation function decays as

$$\langle \boldsymbol{r}_e(t) \cdot \boldsymbol{r}_e(0) \rangle = 4Pe^2 L^3 \left(\frac{L}{l}\right)^3 e^{-\gamma_R t} \sum_{n=1}^{\infty} \frac{\varphi_{2n-1}(L/2)^2}{\hat{\xi}_{2n-1}},$$
(14)

due to the rotational diffusion coefficient of an ABP. The crossover between the two regimes depends on the number of active sites (L/l) along the polymer contour. The relaxation behavior of long polymers, where typically $L/2l_p = L/l \gg 1$, is dominated by the internal polymer dynamics. Note that the relaxation time strongly depends on the activity. Short polymers or polymers with

only a few active sites relax by the rotational diffusion of the active process. The limiting case is a dumbbell of APBs. ⁶⁵ As noticed before³⁵, the decay is slower when the rotational diffusion D_R dominates the decay of the correlation function. ³⁸

4. Dynamics: Mean Square Displacement

The mean square displacement (MSD) $\langle \Delta \mathbf{r}(s,t)^2 \rangle = \langle (\mathbf{r}(s,t) - \mathbf{r}(s,0))^2 \rangle$ of a point $\mathbf{r}(s,t)$ along the polymer contour includes contributions from the polymer center-of-mass motion and displacements with respect to the center of mass. Averaging of the polymer contour yields

$$\langle \overline{\Delta r}(t)^{2} \rangle = \langle \Delta r_{cm}(t)^{2} \rangle + \sum_{n=1}^{\infty} \left[\frac{6k_{B}T\tau_{n}}{\gamma} \left(1 - e^{-t/\tau_{n}} \right) + \frac{2v_{0}^{2}l\tau_{n}^{2}}{1 + \gamma_{R}\tau_{n}} \left(1 - \frac{e^{-\gamma_{R}t} - \gamma_{R}\tau_{n}e^{-t/\tau_{n}}}{1 - \gamma_{R}\tau_{n}} \right) \right].$$
(15)

The center-of-mass contribution is similar to that of an single ${\rm ABP^{1,50}}$

$$\left\langle \Delta \boldsymbol{r}_{cm}(t)^{2} \right\rangle = \frac{6k_{B}T}{\gamma L}t + \frac{2v_{0}^{2}l}{\gamma_{R}^{2}L} \left(\gamma_{R}t - 1 + e^{-\gamma_{R}t} \right) . \tag{16}$$

As a generalization, the total polymer friction γL appears in the contribution of the Brownian motion, and the active term contains L/l, the number of active sites along the polymer contour.³⁶

Figure 5 displays MSDs of flexible and semiflexible polymers. For passive polymers, we find the well-known Rouse dependence \sqrt{t} for flexible polymers⁵⁸ and the dependence $t^{3/4}$ for semiflexible polymers^{66–68} at $t/\tau_1 \ll 1$. In the presence of activity, the diffusivity is significantly enhanced, as already noted before, ^{32,33,64} the more the higher the Péclet number. We can identify three characteristic time regimes. At short times, an activityspecific ballistic regime appears, which is already well pronounced for $Pe \approx 20.^{32,33,64}$ For times $t\gamma_R \approx 1$, the MSD crosses over to a Rouse-type regime (\sqrt{t}) determined by the internal polymer dynamics. Finally, the center-of-mass motion dominates the MSD with a linear increase in time for $t/\tau_1 \gg 1$. It is worth emphasizing that this regime is dominated by activity rather than thermal noise, since $\langle \Delta \mathbf{r}_{cm}(t)^2 \rangle = 2v_0^2 lt/\gamma_R L$. Thereby, the crossover time $t\gamma_R\gtrsim 1$ from the ballistic to the Rouse-type regime shifts to smaller values with increasing Péclet number, a consequence of the decreasing relaxation times τ_n with increasing Pe (Fig. 2). Simultaneously, the polymer characteristic regime $\sim \sqrt{t}$ becomes shorter and vanishes for large Péclet numbers. This shortening is a consequence of the finite extensibility of a polymer and is completely missing in a bare Rouse-model-type approach. 32, 33, 35, 37, 64 However, there is a remarkable feature in the intermediate time regime $1 < \gamma_R t < \gamma_R \tau_1$ for semiflexible polymers. Here, at

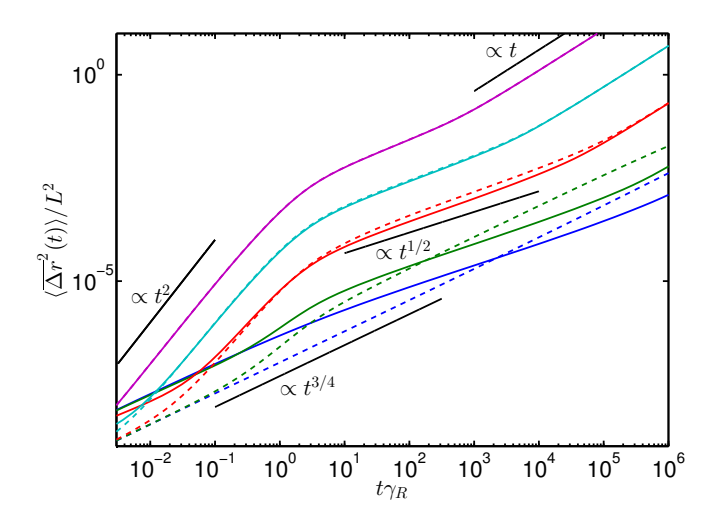


FIG. 5. (Color online) Mean square displacements of a flexible $(L/2l_p=10^3, \text{ solid lines})$ and semiflexible polymer $(L/2l_p=1, \text{ dashed lines})$ for the Péclet numbers Pe=0 (blue), 3×10^0 (green), 2×10^1 (red), 10^2 (cyan), and 5×10^2 (purple) (bottom to top). The time is scaled by the factor $\gamma_R=2D_R$ of the rotational diffusive motion.

sufficiently large Péclet numbers, the segmental MSD of semiflexible polymers exhibits the \sqrt{t} -dependence characteristic for flexible polymers.⁵⁸ This is a consequence of the crossover of the relaxation times from being bending-mode dominated to being Rouse-mode dominated with increasing activity. Such a change does not appear when the stretching coefficient of a passive polymer $(\mu=1)$ is used only. In this case, the $t^{3/4}$ dependence persist for all Pe in the intermediate time regime.

C. Simulations of Passive Polymer in Active Fluid

The properties of a passive polymer embedded in a fluid of active Brownian particles in two dimensions (2d) have been studied by various computer simulations. 30,31,33,39 All studies find significant conformational changes of the polymer due to the active environment in agreement with the above theoretical considerations. In particular, flexible polymers monotonically swell with increasing activity and the probability distribution of the end-to-end vector shifts to large values with increasing activity (v_0) . The scaling behavior of the end-to-end distance with increasing polymer length has been investigated for various activities.³⁰ Simulations predict polymer swelling with an activitydependent scaling exponent larger than the Flory value $(3/4 \text{ in } 2d^{58,69})$ for short polymers. However, for long polymers a crossover to the scaling prediction for selfavoiding passive polymers is obtained. Moreover, the effect of stiffness on the polymer conformations has been considered, 31,33 and a shrinkage with increasing activity been found above a certain stiffness. Moreover, at large

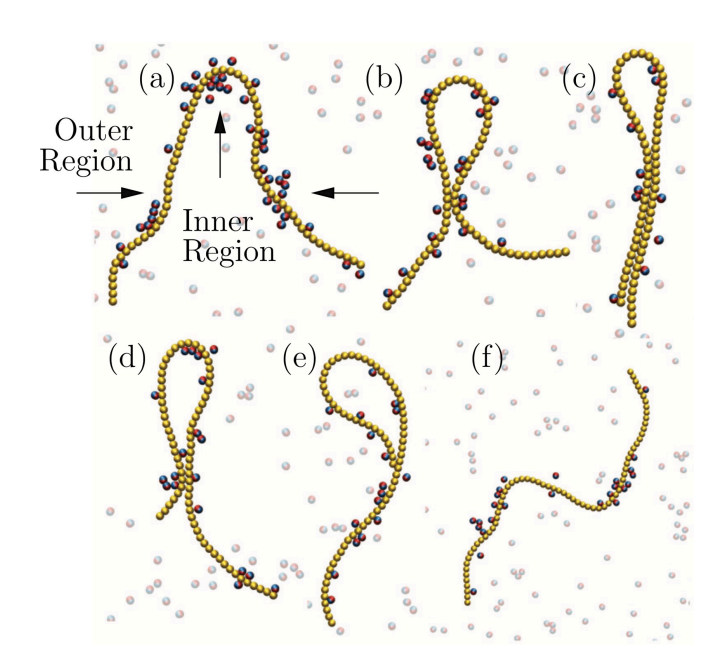


FIG. 6. (Color online) Simulation snapshots of semiflexible polymers embedded in an active fluid at various stages of a folding and unfolding process (a) \rightarrow (f). The propelling force points from the blue to the red hemisphere. Active particles off the filament are displayed semitransparent for clarity. (Reprinted figure with permission from 31 . Copyright 2014 by the American Physical Society.)

activities, flexible and semiflexible polymers exhibit the same conformations.^{31,33} These findings are in agreement with theoretical predictions (Fig. 3). In the 2d studies, the polymers exhibit particular conformations as illustrated in Fig. 6.31,39 An activity-induced bending of the polymer implies an asymmetric exposure to active particles, with more active particles on its outer region (cf. Fig. 6). Simultaneously, the inner ABPs accumulate in regions of highest curvature, as has been observed for ABPs in convinement⁷⁰. The combination of these two effects lead to particular polymer conformations such as hairpins. These structures are only temporarily stable and dissolve and rebuild in the course of time. Hence, the polymer will fluctuate between the two states (hairpin – stretched) in time for certain activities.³¹ Such a behavior cannot be found in the theoretical treatment of Sec. IIB, because there excluded volume interactions are neglected. Certain conformational aspects are a consequence of the 2d character of the system, because for polymers in 3d no such features have been found.³¹ Without doubt, we hardly expect to see conformations as in Fig. 6(c) in 3d with rather parallel strands. However, as show above, semiflexible polymers in 3d also shrink due to active noise.

Considering dynamical aspects, polymer looping, i.e., the formation of rings where the two polymer ends meet, in 2d has been addressed.³³ For flexible chains, the looping probability decreases with increasing activity, which

can be attributed to the swelling of the polymer with increasing activity. For semiflexible polymers, the looping probability shows a non-monotonic dependence on activity—it increases with increasing activity at small activity and decreases at large activity in the same manner as for flexible polymers and independent of stiffness. This is interpreted in terms of two competing effects of the active particles.³³ On the one hand, active noise increase the effective chain flexibility and leads to a polymer shrinkage. On the other hand, activity implies unbinding of end monomers, i.e., breakup of rings. Simultaneously, the looping time, i.e., the time interval between conformations where a polymer end-to-end distance assumes the equilibrium value and subsequently the ends approach their closest allowed distance, decreases substantially with increasing activity. 33 Moreover, the polymer-length dependence of the looping time changes from the power-law $\sim N^{2.7}$ for a passive polymer to $\sim N^{2.3}$ for an active one. This points to a drastically increased relaxation time of the polymers in presence of the active noise in agreement with the theoretical prediction of Sec. IIB.

D. Simulations of a Polymer of Active Brownian Particles

Simulations of polymers composed of active Brownian particles have also been performed, both, for partially active polymers²⁹ as well as fully active ones.³⁴ For a fully active polymer, every monomer is an ABP and independently changes its orientation according to Eq. (2). Additionally, the individual monomers experience bond force and excluded-volume interactions, as passive polymers, as well as the active force $\hat{\gamma}v_0e$. The results indicate that the Flory scaling exponents are also valid in this case, when the chain length increases at a given activity. For an ideal (phantom) chain, activity only affects the prefactor. However, the presence of excluded-volume interactions leads to a non-monotonic chain extension with increasing self-propulsion. First the polymer shrinks and then swells with further increasing activity. The initial shrinkage is attribute to caging of monomers by neighbors. With increasing activity, the monomers are able to escape from the local cage, which leads to a swelling of the polymer. The caging seems to be specific for polymers of ABPs in 2d, because flexible polymers in an active fluid swell with increasing activity rather than shrink (Fig. 3). Moreover, the caging should be far less relevant for active polymers in 3d.

III. SELF-PROPELLED POLAR SEMIFLEXIBLE POLYMERS

The activity of polymer segments (or monomers) is not always randomly oriented, as discussed in Sec. II, but can be correlated along the chain. We focus here on polar active polymers, where the activity is always aligned with the local polarity, *i.e.* which are propelled along their contour by an (external) tangential force. $^{41-45}$ A possible realization are polar active filaments on carpets of molecular motors as in motility assays. 13,40 In simulations, semiflexible filaments are modeled by a series of beads connected by stiff springs (touching bead model) and a bending potential. 44 For self-propulsion, a driving force is added to each bond-vector to uniformly drive the filament along its contour. The overdamped equation of motion of a monomer is then given by

$$\hat{\gamma}\dot{\boldsymbol{r}} = \boldsymbol{F}_t(t) + \boldsymbol{F}(t) + \boldsymbol{\Gamma}(t), \tag{17}$$

where F_t denotes the tangential propulsion force, while F are the bond-stretching and bending forces and Γ random forces due to thermal noise, as defined in Sec. II.

Again, propulsion is characterized by a Péclet number. In contrast to Sec. II, however, the Péclet number Pe is here defined on the polymer length scale as

$$Pe = \frac{v_0 L}{D_t} = \frac{f_p L^2}{k_B T},\tag{18}$$

i.e., by the ratio of the self-advection time L/v_0 and self-diffusion time L^2/D_t . Together with the ratio of persistence length and filament length, the flexure number

$$\mathfrak{F} = \frac{PeL}{l_p} = \frac{f_p L^3}{\kappa} \tag{19}$$

is introduced, which measures the strength of propulsion versus bending.

A. Conformations and Dynamics of Polar Active Polymers

Depending on the ratio of bending rigidity and propulsion strength, three different regimes have be observed (cf. Fig. 7). For weak propulsion, the self-propelled polymer behaves like a passive polymer, except that the relaxation times are shorter ("polymer regime"). As propulsion increases, spiral structures appear transiently ("weak spiral regime"), until, at large propulsion, stable spirals form ("strong spiral regime").

As long as the aspect ratio of the filaments and the interactions between distant segments (excluded volume) do not matter, the (dimensionless) Péclet and flexure numbers completely define the system. However, in spiral states, self-interactions are strong, and details of the polymer discretization can become important. This can be seen by considering the initial state of spiral formation, when the front bead bumps into the middle or rear part of the chain. Then, a strong corrugation of the polymer structure due to the sequence of repulsive spherical beads implies an effective friction, which promotes spiraling. These results suggest that for denser systems and high propulsion forces, models with smoother interactions are more appropriate, e.g., by building the polymer with overlapping beads^{44,71}.

To distinguish the polymer regimes from the spiral regimes, the kurtosis of the spiral number

$$\mathfrak{s} = (\phi(L) - \phi(0))/2\pi,\tag{20}$$

is a convenient order parameter. The spiral number $\mathfrak s$ counts how many times the filament is wrapped around itself, where $\phi(s)$ is the bond orientation at position s along the contour of the filament (cf. Fig. 8). In the polymer regime, a Gaussian distribution of $\mathfrak s$ is observed, resulting in a kurtosis of 3. When spirals occasionally form, a secondary peak appears in the distribution, resulting in an increased kurtosis (cf. Fig. 8). However, when spirals are stable, the distribution is very narrow, resulting in a very small kurtosis. In general, spirals form for large Péclet numbers and small persistence lengths, as displayed quantitatively in Fig. 8.

In the polymer regime, the observed conformations match those at equilibrium, except that the characteristic time scales strongly decrease due to propulsion (Fig. 9). As for the active polymers discussed in Sec. IIB, the relaxation time is found to be inversely proportional to the driving force. This can be understood qualitatively by the "railway motion" of the polymer (Fig. 10). A polymer trajectory resembles again the conformation of an (infinitely long) semiflexible polymer, with the same conformational characteristics as the (passive) polymer itself. The self-propelled polymer is just riding this railway, sampling the conformations as it moves along. Thus, it attains a statistically uncorrelated conformation after a time $l_p/v_0 = l_p\gamma/f_p$. This is consistent with the 1/Pedependence of $\tau_s(q)$ displayed in Fig. 9. The railway motion also explains the observed translational and rotational diffusion coefficients. The polymer (both the propelled filament and the railway trajectory) loose orientational correlation over a length scale determined by the persistence length. Thus, the self-propelled polymer decorrelates, when it travels along the railway, as determined by the tangent-vector correlation function

$$\langle \boldsymbol{t}(s,t) \cdot \boldsymbol{t}(s',0) \rangle = \langle \boldsymbol{t}(s+v_0t,0) \cdot \boldsymbol{t}(s',0) \rangle$$

= $\exp(-(s-s'+v_0t)/l_p)$ (21)

With this correlation function, the diffusion of the end-toend vector orientation can easily be obtained by integration. This gives the active contribution to the rotational diffusion coefficient 44

$$D_{r,a} = v_0/l_p. (22)$$

Figure 11 shows that simulation results for a wide range of persistence lengths nicely collapse onto a single line as predicted by Eq. (22). Note that for flexure numbers \mathfrak{F} larger than about 10^2 , the active contribution clearly dominates the passive diffusion. We want to emphasize that the same behavior of the rotational diffusion coefficient can be expected for sufficiently long tread-milling filaments with high polymerization and depolymerisation rates.

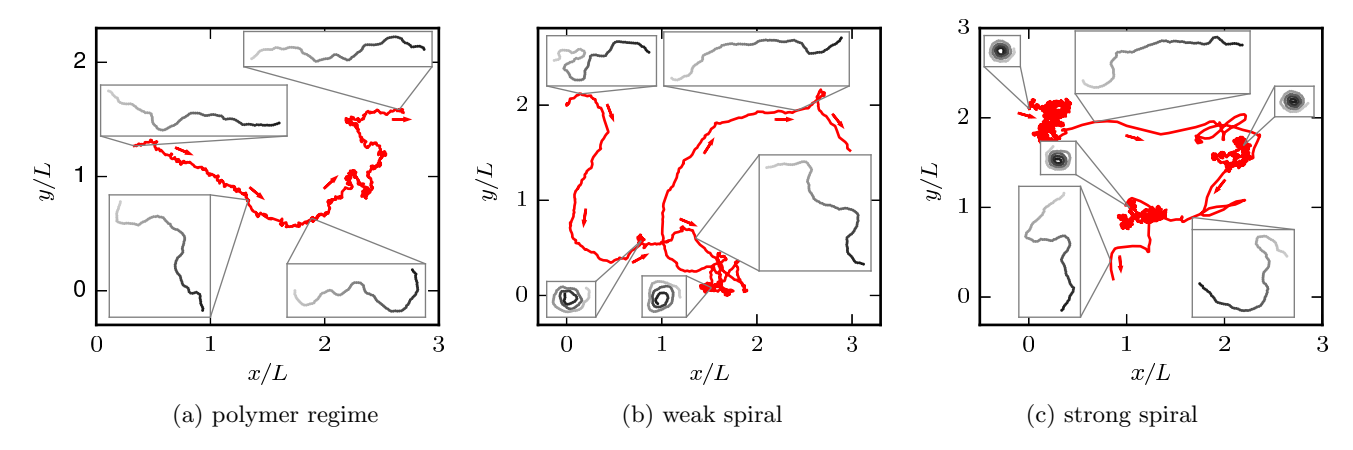


FIG. 7. (Color online) Trajectories of the center of mass of filaments and filament configurations from selected snapshots (insets: grayscale, leading tip black) for $l_p/L = 0.2$ (with N = 100 beads). Arrows point in the direction of movement. (a) At Pe = 200, there is no sign of spiral formation. (b) At Pe = 1000 spirals form occasionally, but the overall behavior is dominated by an elongated chain. (c) At Pe = 5000, the spiral state is predominant. The chain has a directed motion in the elongated state. In the spiral state, the translational motion is almost purely diffusive. This leads to separated clusters in the trajectories for simulations in the strong spiral regime, visible for example in the upper left inset in (c). The length of the depicted trajectories corresponds to approximately 0.13τ (a), 0.13τ (b), and 0.6τ (c), where $\tau = L^3\hat{\gamma}/4k_BT$. (From Ref.⁴⁴ - Published by The Royal Society of Chemistry)

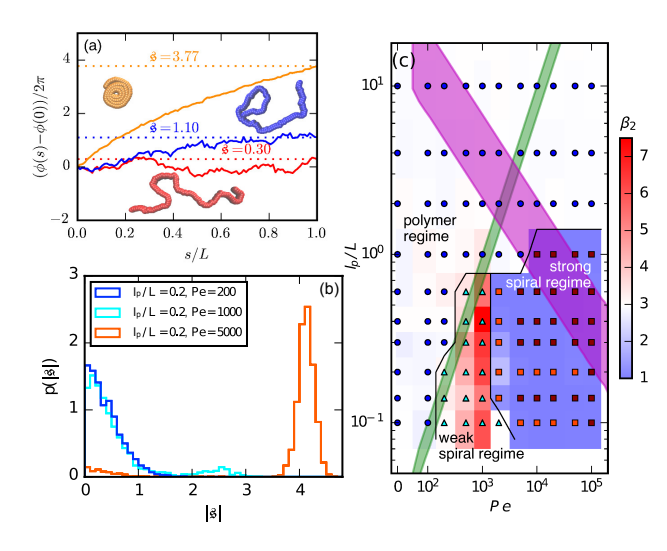


FIG. 8. (Color online) (a) Classification of the filament structure as elongated (red, bottom), weakly wound-up (blue, middle), and strongly wound-up (orange, top) by the spiral number \mathfrak{s} . (b) Probability distribution function $p(|\mathfrak{s}|)$ of the absolute value of the spiral number for three different Péclet numbers. (c) Phase diagram. The kurtosis $\beta_2 = \langle (\mathfrak{s} - \langle \mathfrak{s} \rangle)^4 \rangle / \langle (\mathfrak{s} - \langle \mathfrak{s} \rangle)^2 \rangle^2$ in different regions is indicated by colors. Blue bullets: polymer regime. Cyan triangles: weak spiral regime. Light and dark red squares: strong spiral regime. For the dark red squares, spirals did not break up during the simulations once formed. Black lines are a guide to the eye. Green area (light gray): threshold for spiral stability against break-up by widening. Spirals above this threshold will unfold by widening, spirals below will not. Purple (dark gray): parameter space that can be achieved for actin filaments on a myosin carpet at $T=300\,\mathrm{K}$ using the parameters for f_p and κ of Ref. 72. (From Ref. 44 - Published by The Royal Society of Chemistry)

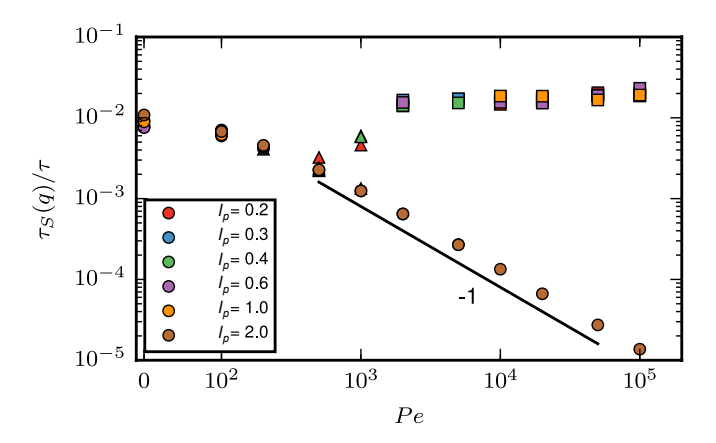


FIG. 9. (Color online) Relaxation time $\tau_S(q)$ of self-propelled filaments for $q\approx 5\pi/L$ and various persistence lengths, with $\tau=\gamma L^3/4k_BT$. Circles correspond to the polymer regime, triangles to the weak spiral regime, and squares to the strong spiral regime. (From Ref. 44 - Published by The Royal Society of Chemistry)

B. Beating of Active Polar Filaments Pushing Against an Obstacle or Load

The situation becomes more complex, when the polymer cannot move freely. If the polymer is fixed at some point, the motion of the filament is restricted, and compression due to the propulsive force builds up. The part of the filament that pulls away from the fixation point is obviously pulled to a straight configuration under tension. The situation becomes more interesting on the pushing side, where the propulsive forces add up and lead to a large compressive stress. Similar to an elastic rod under compressive load, 73-75 this (inhomogeneous)

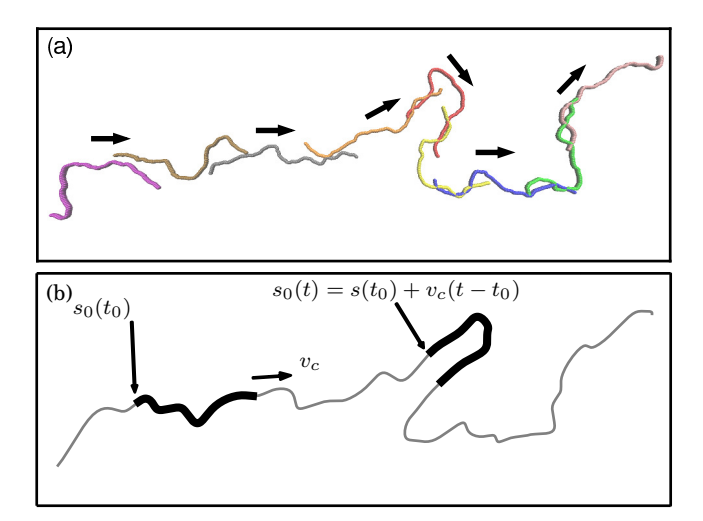


FIG. 10. (Color online) (a) Series of snapshots of a filament with $l_p/L = 0.3$ (N = 100 beads) and Pe = 1000. The filament moves along its contour superimposed with thermal motion. Subsequent filaments are represented by different colors for better differentiation. (b) Idealized railway motion in the absence of thermal motion. The filament (thick black line) moves with velocity v_0 along the contour of an infinite chain with the same l_p (gray line). $s_0(t)$ runs along the contour of the infinite chain and marks the end point of the filament. (From Ref. 44 - Published by The Royal Society of Chemistry)

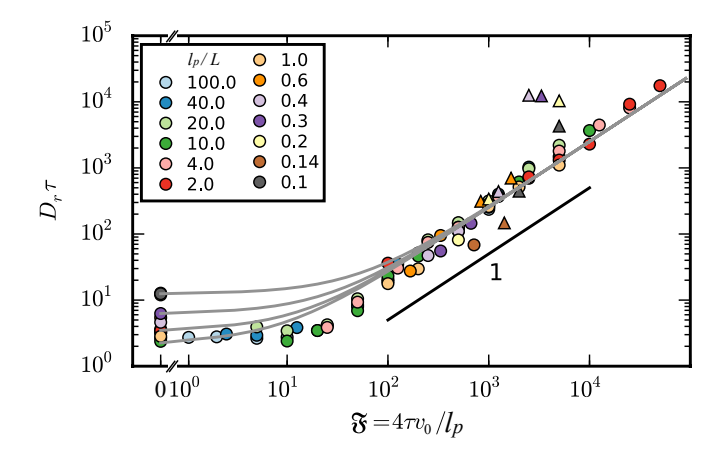


FIG. 11. (Color online) Rotational diffusion coefficient D_r as a function of the flexure number \mathfrak{F} , with $\tau = \gamma L^3/4k_BT$. Symbol shapes indicate the region in the phase diagram: circle: polymer regime; triangle: weak spiral regime. Gray lines are analytical predictions from the "railway assumption" for different passive rotation diffusion constants $D_{r,p}$. (From Ref. ⁴⁴ - Published by The Royal Society of Chemistry)

compressive stress can lead to buckling.

To understand the buckling of active filaments, two cases are considered independently. A pinned filament is fixed at one end point, but free to rotate, while a clamped filament is fixed in its orientation at the fixation point as well. Linear stability shows, at low temperature, that a pinned filament will buckle if the flexure number exceeds a critical value $\mathfrak{F}_c^{rot} = 30.6^{72}$. The filament will spon-

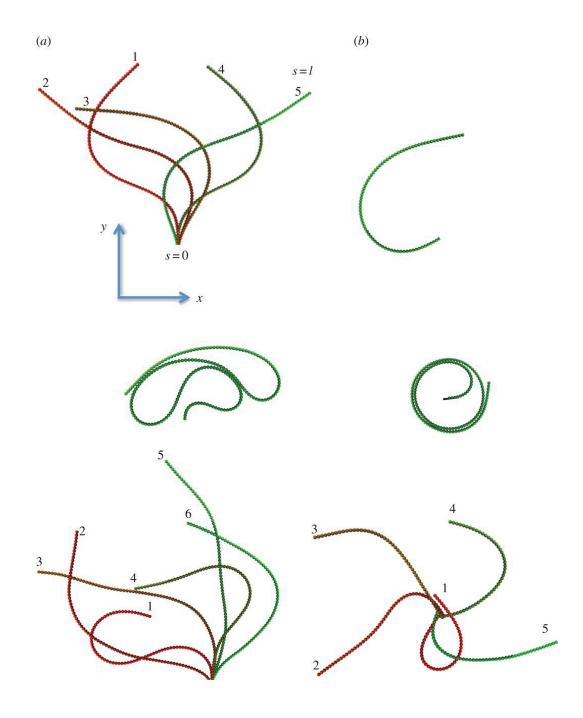


FIG. 12. (Online color) Dynamical shapes of anchored active polar filaments. (a) Filaments clamped at one end exhibit beating patterns. Short filaments show regular beating (top), contacting looped shapes are observed for longer polymers (middle), and for strong noise highly erratic shapes are obtained (bottom). (b) Filament with an anchored but freely rotating end show spirals. Short filaments at weak noise rotate with a constant frequency (top), longer filaments rotate as tightly wound spirals (middle), erratic motion without a defined shape or rotation frequency appear for strong noise (bottom). (From Ref. 43, by permission of the Royal Society)

taneously break the symetry, and bend in one direction, leading to rotating motion around the pinning point. A similar instability analysis for a driven clamped filament shows a Hopf-type instability at the critical flexure number $\mathfrak{F}_c^{rot} = 75.5$, leading to beating motion⁷².

Beyond linear stability, one has to resort to computer models and numerical solutions and simulations 43 . These studies confirm the results of linear-stability analysis, and predict a rich variety of dynamic states beyond the stability threshold as illustrated in Fig. 12. Furthermore, the simulations reveal a power-law scaling of beating and rotation frequencies for pinned and clamped filaments, respectively. In both cases, the frequency is predicted to scale with the 4/3 power of the propulsive force, *i.e.*, $\omega \sim f_p^{4/3}$.

A system intermediate between free-swimming and clamped or tethered filaments is filaments pushing a finite-size load at the front end of the filament. A tiny load is equivalent to a free-moving filament, a huge load corresponds to a clamped filament. Here, it is important to note that the size and shape of the load together determine the translational and rotational friction of the load; high and low rotational frictions imply beating and

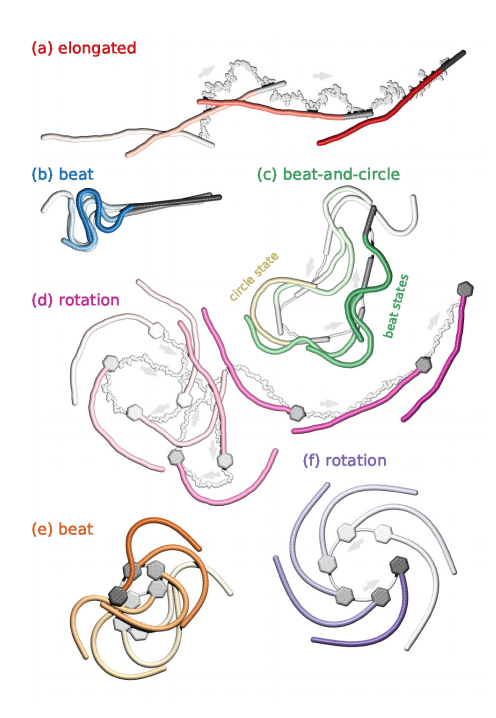


FIG. 13. (Online color) Sequence of filament snapshots from the different regimes. Time increases from transparent to opaque. The gray lines are the trajectories of the center of mass of the rigid body. (a) Filament attached to a rodshaped load in the elongated phase with $\mathfrak{F} = 50$, $l_p/L = 2$, and $\gamma_F/\gamma_B = 5$; γ_F and γ_B are the friction coefficient of the filament and the body, respectively. (b) Filament attached to a rod-shaped load in the beat phase with $\mathfrak{F} = 5000$, $l_p/L = 2$, and $\gamma_F/\gamma_B = 1.67$. (c) Filament attached to a rod-shaped load in the beat-and-circle regime with $\mathfrak{F}=5000,\ l_p/L=2,$ and $\gamma_F/\gamma_B = 5$. (d) Filament with a hexagonal head in the rotation phase with $\mathfrak{F} = 250$, $l_p/L = 2$, and $\gamma_F/\gamma_B = 1.64$. (e) Filament with a hexagonal head in the beat phase at low thermal noise with $\mathfrak{F} = 1000$, $l_p/L = 2000$, and $\gamma_F/\gamma_B = 1.1$. (f) Filament with a hexagonal head in the rotation phase at low thermal noise with $\mathfrak{F} = 150$, $l_p/L = 2000$. (From Ref. 45 -Published by The Royal Society of Chemistry)

rotational dynamics, respectively. Accordingly, different dynamic regimes are obtained depending on the size and shape of the load, as well as elasticity and driving force of the filament (cf. Figs. 13 and 14). For small driving forces and small loads, the filament is elongated and a buckling transition occurs at a well-defined combination of driving force and load size. Again, this threshold can be understood from a linear stability analysis of the overdamped equations of motion of a filament attached to an aligned rod. 45,76. For sufficiently strong propulsion, the filament turns from a stable node, where all eigenvalues of the Jacobian matrix are real and negative (with the exception of the zero eigenvalues that correspond to Goldstone modes), to a stable focus, where the real parts of the eigenvalues are negative but at least one pair of complex conjugated eigenvalues with a non-zero imaginary part exists; in the latter case, these modes are not unstable, but show enhanced fluctuations. Beyond a higher

critical flexure number, unstable modes appear, leading to buckling of the filament. The critical flexure number depends on the size of the load, but converges for large loads to the critical flexure number for clamped filaments $\mathfrak{F}_c^{rot}=75.5$. Noise broadens this transition and permits amplification of further modes. For low noise and large load, the results for clamped filaments are recovered.

These buckling transitions to beating and rotating motion have a profound effect on possible applications. A longer filament results in a larger propulsion force on the load, however, if this propulsive force is large enough for the filament to buckle, it enters a less- or non-propulsive state. Thus, optimal propulsion can be expected just below the critical line.

IV. HYDRODYNAMICS AND ACTIVE POLYMERS

Swimming microorganisms or synthetic self-propelled particles are often embedded in a fluid and hydrodynamics is essential for their dynamics and the propulsion itself. Consequently, theoretical³⁵ and simulation^{46–49} studies have been performed to unravel the influence of hydrodynamic interactions on the dynamics of active polymers. Thereby, different routes have been taken. On the one hand, activity is considered as an external driving force 35,46,47 and hydrodynamic interactions are taken into account on the level of a hydrodynamic tensor, either the Oseen^{58,77} or the Rotne-Prager-Yamakawa tensor. 77,78 On the other hand, polymers comprised of energy-converting active monomers are considered. 48,49 where propulsion is achieved by the hydrodynamic flow generated by those monomers. In a theoretical description, with a representation of the active particle by a spherical colloid, propulsion is attained by a prescribed velocity on the colloid surface. A prominent example for such an active colloid is the squirmer model, ^{79,80} which is a generic model for a broad class of microswimmers, ranging from diffusiophoretic particles to biological cells. 81-84 For a spherical squirmer, the surface flow field (slip velocity) is given by

$$\mathbf{v}_{sq} = B_1 \sin \vartheta (1 + \beta \cos \vartheta) \mathbf{e}_{\vartheta} \tag{23}$$

(cf. Fig. 15 for the definition of the angle ϑ and the tangential vector \mathbf{e}_{ϑ}). The coefficient $B_1=2U_0/3$ is related to the swimming velocity U_0 of the squirmer and β accounts for the strength of the force dipole. Thereby $\beta>0$ for a puller, $\beta<0$ for a pusher, and $\beta=0$ for neutral swimmer. Figure 15 displays flow fields for pullers, pushers, and neutral squirmers.

The far field of pullers and pushes is dominated by the force dipole contribution and decays as $1/r^2$ with distance from the colloid center. The source dipole field dominates for neutral squirmers and decays as $1/r^3$. Note that an active particle is force and torque free and, hence, no Stokeslet term is present. In an active polymer, such colloids are arranged in a linear fashion. The respective bond forces, or other intramolecular forces, give rise to a

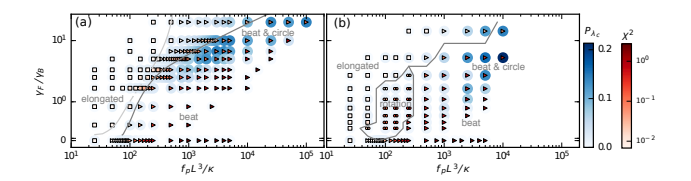


FIG. 14. (Online color) Phase diagram of the various filament conformations as a function of the ratio between the head size and filament length γ_F/γ_B and the flexure number $\mathfrak{F}=f_pL^3/\kappa$. (a) Filament with rod-shaped load at high temperature $(l_p/L=2)$. Symbols: triangles for oscillations in C_{λ_1} , circles for persistent rotation, double-circles for rotation with alternating directions, squares for non-rotating and non-oscillating states. The gray line in (b) is a phase boundary and a guide to the eye. The gray line in (a) indicates the transition from a stable focus to an unstable focus in the stability analysis. The light gray line markes the transition from a stable node to a stable focus. The line is dotted where the transition from a node to a focus is interpolated because it could not be determined accurately due to numeric difficulties. P_{λ_C} is the fraction of states in which the circle mode ψ_c dominates, and χ^2 measures the deviation from a Gaussian behavior of λ_1 and λ_2 . (From Ref. 45 - Published by The Royal Society of Chemistry)

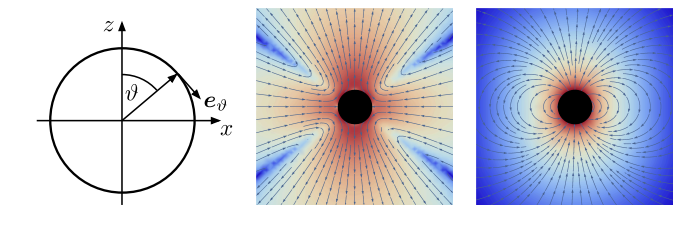


FIG. 15. (Online color) Definition of the angle ϑ on the squirmer surface (left) and flow streamlines of isolated squirmers in the swimmer reference frame for a pusher (middle) and a neutral squirmer (right). For a puller, the flow lines in the left figure have to be inverted.

Stokeslet-type hydrodynamic flow field, which decays as 1/r.

Expression for the translation and rotation of spherical active particles are derived in Refs. ^{49,85} in terms of mobility matrices. Aside from the well-known matrices ^{77,86,87} for passive particles, extension are provided for active particles that relate the modes of the nonequilibrium surface velocity to their rigid body motion. The rather general approach allows for the study of motile and non-motile systems taking into account fundamental solutions of the Stokes equation up to the desired order.

A. Polar Semiflexible Filaments and Hydrodynamic Interactions

A model, which is closely related to that described in Sec. III A, has been employed for the motion of polar semiflexible filaments in a fluid.⁴⁶ Three main regimes of motion have been detected, which are denoted as translation, snaking, and rotation. The appearance of the respective type of motion depends on the polymer stiffness, but is independent of the absence or presence of hydrodynamic interactions. Although the behavior is qualitatively similar, hydrodynamic interactions yield a significant quantitative difference. Specifically the parameter range of rotation, where a filament moves in a circular

fashion, increases considerably in the presence of hydrodynamic interactions.

The collective motion of actin filaments driven by molecular motors has been studied experimentally in motility assays. ^{13,19,40} The results are controversial, hydrodynamic interactions are considering either to be essential for the observed structure formation, ^{13,40} or hydrodynamic interactions are judged as irrelevant and the phenomenon is attributed to direct contacts between the filaments. ¹⁹ Simulations ⁴⁶ show that both interactions lead to collective motion of semiflexible polymers. Only the parameter ranges for rotational motion are rather different and hydrodynamic interactions enhance rotational motion at weak active forces. The amplification and initiation of rotational motion by hydrodynamic interactions has also been demonstrated for two filaments. ⁴⁷

B. Hydrodynamically Induced Oscillations of Filaments

A semiflexible polymer, when clamped at one of its ends and whose monomers generate a dipolar flow field (force dipole) tangential to the polymer, exhibits spontaneous oscillations when activity exceeds a threshold. Here, simulations yield two distinct filament motions. For intermediate activities, a corkscrew-type rotation is found in three dimensions. For large activities, the filament beats in a plane with waves propagating from the clamp to the filament tip. A detailed investigation shows that this beating originates from hydrodynamic interactions and that there is no beating without it. 88

The beating motion itself and the respective beat patterns are different from those described in Sec. IIIB, since the monomers possess a force dipole only and no self-propulsion velocity. In contrast, the polymers of Sec. IIIB are propelled along the tangent of the polymer. Evidently, the latter can stimulate other motion patterns. It remains to analyse how propulsion modifies the motion of the filaments in presence of hydrodynamic interactions and a force dipole.

Similar to the studies of Sec. IIIB the transport of a load by a hydrodynamically-active filament has been

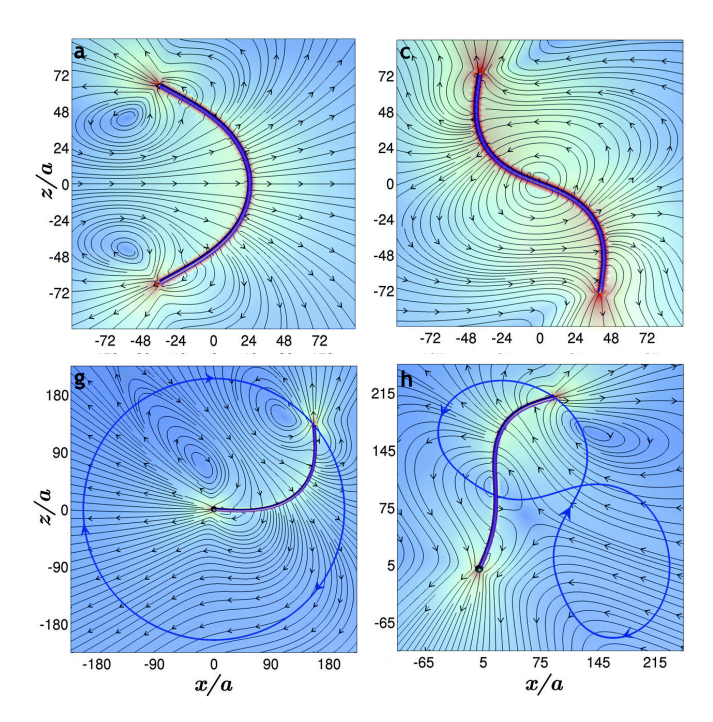


FIG. 16. (Online color) Flow streamlines of nonequilibrium steady-state conformations of free ((a), (c)) and tethered ((g), (h)) filaments at various activities. The activity increases from left to right. The snapshots show the first two excited elastic modes, where the filament in (a) is translating and that in (c) rotating. For the tethered filament, a rotation is obtained first and an oscillating state at higher activity. (Reproduced in part from Ref. 49 with permission of The Royal Society of Chemistry.)

studied.⁸⁹ Five distinct beating modes have been identified giving rise to transport. Two of them appear due to the load and are not present for clamped filaments.

C. Hydrodynamic Instabilities and Filament Dynamics

Applying the same type of model, the dynamics of free and tethered (fixed, but freely rotating end) active filaments has been analyzed.⁴⁹ Considering the flow fields of polymers comprised of extensile (pusher) and contractile (puller) (cf. Fig. 15) monomers, leads to the conclusion that flow compresses contractile and extends extensile filaments. This is evident from the flow profiles of the monomers displayed in Fig. 15. For pushers, subsequent monomers are repelled by their flow fields, whereas for pullers the monomers are attracted. Hence, for a symmetrically curved polymer, active flow preferentially suppresses bending of contractile filaments, but enhances it for extensile filaments. Thus, the interplay between flow and bending leads to a destabilization of straight extensile filaments, whereas contractile filaments are stabilized.⁴⁹

Looking at extensile polymers only, a wide spectrum of nonequilibrium stationary states appear. A selection is

displayed in Fig. 16 for free and tethered filaments. 49 At a critical activity, a linear instability occurs and a straight free filament bends and assumes a U-shaped form. As is illustrated by the flow field (Fig. 16(a)), the polymer moves then autonomously although the self-propulsion velocity U_0 is zero. With increasing activity, higher elastic modes appear via a serious of bifurcations (Fig. 16(c)). Thereby, asymmetric conformations with respect to the center exhibit a rotational motion. Note that the force dipoles are tangential to the polymer contour. Filaments tethered by one of their ends (Fig. 16(g), (h)) exhibit a rotational motion above a threshold activity. An increasing activity leads to flagella-like beating (Fig. 16(h)). For even larger activities, filaments with more bend conformations appear, which rotated again. For even higher activity, conformations with higher elastic eigenmodes are expected, which either oscillate or rotate⁴⁹. In general, the filaments move in a plane determined by the initial condition, although the systems is three dimensional.

As mentioned before, a filament is propelled crooked to its tangent even at zero self-propulsion velocity due to the bending of the filament. Correspondingly, the center-of-mass velocity is proportional to the filament curvature and activity. Similarly, this proportionality holds for the rotation frequency about the center-of-mass. ⁴⁹ Hence, motility can emerge due to the hydrodynamic coupling of various active units combined with symmetry broken structures.

V. ACTIVE POLYMERS IN NETWORKS AND DENSE POLYMER SOLUTIONS

A. Viscoelasticity of Dense Solutions of Polar Semiflexible Polymers

In a theoretical study of polar active filaments, the viscoelastic properties of a solution of such polymers (3d) have been analysed.⁴¹ Thereby, significant activityinduced modifications of the passive polymer dynamics have been found. Specifically, the short-time and terminal relaxation times are changed. Increased fluctuations of the longitudinal modes imply a hardening of the solution at high frequencies. Moreover, new relaxation regimes appear due to a change of the ratio between the transverse and longitudinal fluctuations. Specifically, at short times the shear modulus G(t) of the solutions shows new time regimes with the power-law $t^{-1/8}$ followed by a regime $\sim t^{-1/2}$ instead of the semiflexible-polymertypical regime $\sim t^{-3/4}$. Similar to passive polymers, a plateau appears at longer times due to entanglements. For active filaments, this plateau is shorter, both, for rodlike and flexible polymers. Hence, activity leads to a softening or fluidization of the solution due to their directed motion.⁴¹ Similarly, softening for whole cells due to motor activity has been observed.⁹⁰

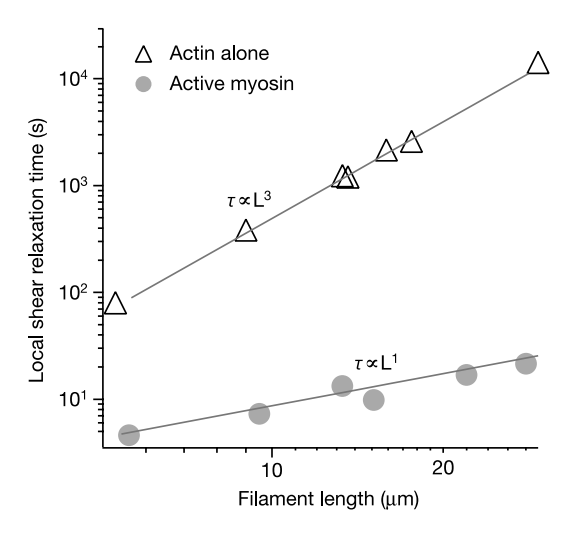


FIG. 17. (Online color) Dependence of the shear relaxation time on filament length for actin and actin-myosin networks. The triangles indicate the relaxation times of an entangled Factin solution, whereas bullets correspond to actin networks with active myosin under ATP conditions. (Reprinted by permission from Macmillan Publishers Ltd: Nature⁹¹, copyright 2002.)

B. Relaxation and Transport Properties

Fluidization of actin-myosin gels due to motor activity has been found experimentally. 91,92 This is particularly interesting, because passive (no ATP) myosin acts as a crosslinker for actin polymers. Accordingly, the storage modulus increases six-fold if passive myosin is added to the solution. However, with a sufficient concentration of ATP, the myosin proteins act as directional motors, and propel the filaments relative to each other, causing a decrease of the relaxation time and fluidization of the gel. Indeed, experiments show a drastic decrease of the viscous relaxation time⁹¹ in qualitative agreement with the theoretical considerations of Sec. IIB. Simultaneously, the length dependence of the relaxation time changes from a L^3 dependence to a linear dependence, as shown in Fig. 17. The linear dependence on actin-length of the relaxation time is in agreement with predictions for the polar active polymer dynamics of Sec. III A (cf. Fig. 9). In contrast, the longest relaxation time of the polymer with APB monomers exhibits a different length dependence, namely $L^3 - L^{2.5}$. This suggests that the actin filaments are indeed driven tangential to their contour.

Recently, the dynamics of different genomic regions in the nucleus of live cells has been studied, in particular, the influence of the protein laminA. ⁹³ LaminA is considered to be important for the organization of chromatin in the cell nucleus by forming or initiating chromosomal interchain interactions (crosslinks between chromatin strands) over the whole nucleus. ⁹³ Measurements of the dynamics of various genomic loci in several cell lines ⁹³ yield, in the presence of laminA, a polymer-like subdiffusive time dependence of the MSD, although with

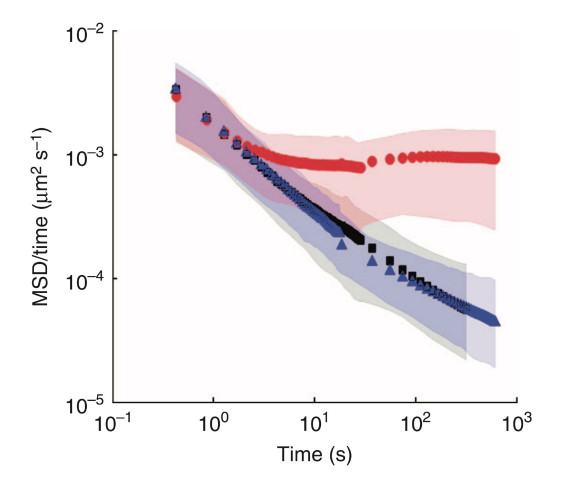


FIG. 18. (Online color) Mean square displacements divided by time for telomeres in Lmna^{+/+} cells (black squares) and Lmna^{-/-} cells (red bullets). Symbols designate the average locus MSD while shaded areas mark the standard deviation of all single loci MSDs. (From Ref.⁹³)

an exponent somewhat smaller than the Rouse value 1/2 (cf. Sec. II B 4). 93 The difference in the exponent can be attributed to viscoelastic effects. 37,64 Depletion of laminA drastically accelerates the dynamics and the MSD crosses over to normal diffusion (cf. Fig. 18). This increase can be attributed to a release of constraints due to the depletion of laminA and appearing large-scale motions of genomic regions, driven by thermal and active noise. 37,93 The transition from a polymer-dynamics-dominated time regime to accelerated diffusion is consistent with our results shown in Fig. 5. Already moderate active noise leads to an accelerated dynamics over several orders in time.

VI. SUMMARY AND OUTLOOK

Polymers and semiflexible filaments are ubiquitous, both in biology and in technical applications. Similar omnipresent is activity in biological systems. However, the implication of an active environment on the polymer properties have only be realized recently, specifically in the context of biological cells. The action of motor proteins, as well as treadmilling due to polymerization and de-polymerization of polar active filament in the cytoskeleton has long been studied to unravel cell motility and internal cell dynamics. Yet, little is know about the effect of the active cell environment on the properties of other contained polymers such as the chromatin. Even less is known about the material properties of active polymer solutions and melts. We think that the incorporation of activity in polymer materials may be a promising route to the design of novel switchable and smart materials.

We are only at the beginning of a detailed understanding of the interplay of driving forces, passive and active noise, polymer flexibility, and constraints due to other polymers or geometrical boundaries. Most studies so far have focused on single filaments, as reviewed in this article. Besides, considerable effort has been devoted to studies of the dynamics of dense systems in two dimensions in the nematic phase. Here, continuum models based on the nematic order parameter proofed to be extremely successful. It will be very interesting in the future to bridge the gap between these very different levels of description, and to connect the single polymer properties to the emergent behavior at large length- and time-scales.

ACKNOWLEDGMENTS

We thank O. Duman, T. Eisenstecken, A. Ghavami, R. Isele-Holder, J. Jäger, A. Mair, G. Saggiorato, and M. Theers for enjoyable collaborations and stimulating discussions. We gratefully acknowledge partial support from the DFG within the priority program SPP 1726 on "Microswimmers – from Single Particle Motion to Collective Behaviour". A computing-time grant on the supercomputer JURECA at Jülich Supercomputing Centre (JSC) is thankfully acknowledged.

- ¹J. Elgeti, R. G. Winkler, and G. Gompper: Rep. Prog. Phys. **78** (2015) 056601.
- ²C. Bechinger, R. Di Leonardo, H. Löwen, C. Reichhardt, G. Volpe, and G. Volpe: Rev. Mod. Phys. 88 (2016) 045006.
- $^3\mathrm{T.}$ Vicsek and A. Zafeiris: Phys. Rep. $\mathbf{517}$ (2012) 71.
- ⁴E. Lauga and T. R. Powers: Rep. Prog. Phys. **72** (2009) 096601.
- ⁵S. Ramaswamy: Annu. Rev. Cond. Mat. Phys. **1** (2010) 323.
- ⁶H. C. Berg: E. Coli in Motion (Biological and Medical Physics Series. Springer, New York, 2004), Biological and Medical Physics Series.
- $^7\mathrm{F.}$ J. Nédélec, T. Surrey, A. C. Maggs, and S. Leibler: Nature $\mathbf{389}$ (1997) 305.
- ⁸J. Howard: Mechanics of motor proteins and the cytoskeleton (Sinauer Associates Sunderland, MA, 2001).
- ⁹K. Kruse, J. F. Joanny, F. Jülicher, J. Prost, and K. Sekimoto: Phys. Rev. Lett. **92** (2004) 078101.
- $^{10}\mathrm{A.~R.}$ Bausch and K. Kroy: Nat. Phys. **2** (2006) 231.
- ¹¹F. Jülicher, K. Kruse, J. Prost, and J.-F. Joanny: Phys. Rep. 449 (2007) 3.
- ¹²Y. Harada, A. Noguchi, A. Kishino, and T. Yanagida: Nature 326 (1987) 805.
- ¹³V. Schaller, C. Weber, C. Semmrich, E. Frey, and A. R. Bausch: Nature **467** (2010) 73.
- ¹⁴J. Prost, F. Jülicher, and J.-F. Joanny: Nat. Phys. **11** (2015) 111.
- ¹⁵H. S. Muddana, S. Sengupta, T. E. Mallouk, A. Sen, and P. J. Butler: J. Am. Chem. Soc. **132** (2010) 2110.
- ¹⁶K. K. Dey, S. Das, M. F. Poyton, S. Sengupta, P. J. Butler, P. S. Cremer, and A. Sen: ACS Nano 8 (2014) 11941.
- ¹⁷M. C. Marchetti, J. F. Joanny, S. Ramaswamy, T. B. Liverpool, J. Prost, M. Rao, and R. A. Simha: Rev. Mod. Phys. 85 (2013) 1143
- ¹⁸A. Cordoba, J. D. Schieber, and T. Indei: RSC Adv. 4 (2014) 17935.
- ¹⁹Y. Sumino, K. H. Nagai, Y. Shitaka, D. Tanaka, K. Yoshikawa, H. Chate, and K. Oiwa: Nature 483 (2012) 448.
- ²⁰C. P. Brangwynne, G. H. Koenderink, F. C. MacKintosh, and D. A. Weitz: J. Cell. Biol. **183** (2008) 583.
- ²¹C. P. Brangwynne, G. H. Koenderink, F. C. MacKintosh, and D. A. Weitz: Phys. Rev. Lett. **100** (2008) 118104.

- ²²C. A. Weber, R. Suzuki, V. Schaller, I. S. Aranson, A. R. Bausch, and E. Frey: Proc. Natl. Acad. Sci. USA 112 (2015) 10703.
- ²³S. C. Weber, A. J. Spakowitz, and J. A. Theriot: Proc. Natl. Acad. Sci. USA **109** (2012) 7338.
- ²⁴A. Javer, Z. Long, E. Nugent, M. Grisi, K. Siriwatwetchakul, K. D. Dorfman, P. Cicuta, and M. Cosentino Lagomarsino: Nat. Commun. 4 (2013) 3003.
- ²⁵A. Zidovska, D. A. Weitz, and T. J. Mitchison: Proc. Natl. Acad. Sci. USA **110** (2013) 15555.
- ²⁶ J. Yan, M. Han, J. Zhang, C. Xu, E. Luijten, and S. Granick: Nat. Mat. **15** (2016) 1095.
- ²⁷R. Di Leonardo: Nat. Mat. **15** (2016) 1057.
- ²⁸Y. Sasaki, Y. Takikawa, V. S. R. Jampani, H. Hoshikawa, T. Seto, C. Bahr, S. Herminghaus, Y. Hidaka, and H. Orihara: Soft Matter 10 (2014) 8813.
- ²⁹D. Loi, S. Mossa, and L. F. Cugliandolo: Soft Matter 7 (2011) 10193.
- ³⁰A. Kaiser and H. Löwen: J. Chem. Phys. **141** (2014) 044903.
- ³¹ J. Harder, C. Valeriani, and A. Cacciuto: Phys. Rev. E **90** (2014) 062312.
- ³²A. Ghosh and N. S. Gov: Biophys. J. **107** (2014) 1065.
- ³³ J. Shin, A. G. Cherstvy, W. K. Kim, and R. Metzler: New J. Phys. **17** (2015) 113008.
- ³⁴A. Kaiser, S. Babel, B. ten Hagen, C. von Ferber, and H. Löwen: J. Chem. Phys. **142** (2015) 124905.
- ³⁵N. Samanta and R. Chakrabarti: J. Phys. A: Math. Theor. **49** (2016) 195601.
- ³⁶T. Eisenstecken, G. Gompper, and R. G. Winkler: Polymers 8 (2016) 304.
- $^{37}\mathrm{\grave{D}}.$ Osmanovic and Y. Rabin: Soft Matter 13 (2017) 963.
- ³⁸T. Eisenstecken, G. Gompper, and R. G. Winkler: J. Chem. Phys. **146** (2017) 154903.
- ³⁹N. Nikola, A. P. Solon, Y. Kafri, M. Kardar, J. Tailleur, and R. Voituriez: Phys. Rev. Lett. **117** (2016) 098001.
- ⁴⁰V. Schaller, C. Weber, E. Frey, and A. R. Bausch: Soft Matter 7 (2011) 3213.
- ⁴¹T. B. Liverpool, A. C. Maggs, and A. Ajdari: Phys. Rev. Lett. 86 (2001) 4171.
- ⁴²Z. Farkas, I. Derenyi, and T. Vicsek, Dynamics of Actin Filaments in Motility Assays, Structure and Dynamics of Confined Polymers, Vol. 87, p. 327. Springer, Netherlands, 2002.
- ⁴³R. Chelakkot, A. Gopinath, L. Mahadevan, and M. F. Hagan: J. R. Soc. Interf. **11** (2014) 20130884.
- ⁴⁴R. E. Isele-Holder, J. Elgeti, and G. Gompper: Soft Matter 11 (2015) 7181.
- ⁴⁵R. E. Isele-Holder, J. Jager, G. Saggiorato, J. Elgeti, and G. Gompper: Soft Matter **12** (2016) 8495.
- ⁴⁶H. Jiang and Z. Hou: Soft Matter **10** (2014) 1012.
- $^{47}\mathrm{H}.$ Jiang and Z. Hou: Soft Matter $\mathbf{10}$ (2014) 9248.
- ⁴⁸G. Jayaraman, S. Ramachandran, S. Ghose, A. Laskar, M. S. Bhamla, P. B. S. Kumar, and R. Adhikari: Phys. Rev. Lett. **109** (2012) 158302.
- ⁴⁹A. Laskar and R. Adhikari: Soft Matter **11** (2015) 9073.
- ⁵⁰J. R. Howse, R. A. L. Jones, A. J. Ryan, T. Gough, R. Vafabakhsh, and R. Golestanian: Phys. Rev. Lett. **99** (2007) 048102.
- ⁵¹F. Peruani, L. Schimansky-Geier, and M. Bär: Eur. Phys. J. Spec. Top. **191** (2010) 173.
- ⁵²P. Romanczuk, M. Bär, W. Ebeling, B. Lindner, and L. Schimansky-Geier: Eur. Phys. J. Spec. Top. **202** (2012) 1.
- ⁵³Y. Fily and M. C. Marchetti: Phys. Rev. Lett. **108** (2012) 235702.
- ⁵⁴J. Bialké, T. Speck, and H. Löwen: Phys. Rev. Lett. **108** (2012) 168301.
- ⁵⁵G. S. Redner, M. F. Hagan, and A. Baskaran: Phys. Rev. Lett. 110 (2013) 055701.
- ⁵⁶B. ten Hagen, R. Wittkowski, D. Takagi, F. Kümmel, C. Bechinger, and H. Löwen: J. Phys.: Condens. Matter 27 (2015) 194110.
- ⁵⁷M. C. Marchetti, Y. Fily, S. Henkes, A. Patch, and D. Yllanes:

- Curr. Opin. Colloid Interface Sci. 21 (2016) 34.
- ⁵⁸M. Doi and S. F. Edwards: The Theory of Polymer Dynamics (Clarendon Press, Oxford, 1986).
- ⁵⁹M. Raible and A. Engel: Appl. Organometal. Chem. **18** (2004) 536.
- ⁶⁰R. G. Winkler, A. Wysocki, and G. Gompper: Soft Matter **11** (2015) 6680.
- ⁶¹R. G. Winkler, P. Reineker, and L. Harnau: J. Chem. Phys. **101** (1994) 8119.
- ⁶²L. Harnau, R. G. Winkler, and P. Reineker: J. Chem. Phys. **104** (1996) 6355.
- ⁶³L. Harnau, R. G. Winkler, and P. Reineker: J. Chem. Phys. **106** (1997) 2469.
- ⁶⁴H. Vandebroek and C. Vanderzande: Phys. Rev. E **92** (2015) 060601.
- ⁶⁵R. G. Winkler: Soft Matter **12** (2016) 3737.
- $^{66}\mathrm{E}$. Farge and A. C. Maggs: Macromolecules **26** (1993) 5041.
- ⁶⁷E. P. Petrov, T. Ohrt, R. G. Winkler, and P. Schwille: Phys. Rev. Lett. **97** (2006) 258101.
- $^{68}{\rm R.~G.~Winkler:~J.~Chem.~Phys.~{\bf 127}}~(2007)~054904.$
- ⁶⁹P.-G. de Gennes: Scaling Concepts in Polymer Physics (Cornell University, Ithaca, 1979).
- ⁷⁰Y. Fily, A. Baskaran, and M. F. Hagan: Soft Matter **10** (2014) 5609.
- $^{71}\mathrm{M.}$ Abkenar, K. Marx, T. Auth, and G. Gompper: Phys. Rev. E 88~(2013)~062314.
- ⁷²K. Sekimoto, N. Mori, K. Tawada, and Y. Y. Toyoshima: Phys. Rev. Lett. **75** (1995) 172.
- ⁷³L. D. Landau and E. M. Lifshitz: *Theory of Elasticity* (Pergamon, New York, 1986).
- ⁷⁴J. Wilhelm and E. Frey: Phys. Rev. Lett. **77** (1996) 2581.
- ⁷⁵R. Chelakkot, R. G. Winkler, and G. Gompper: Phys. Rev. Lett. 109 (2012) 178101.
- ⁷⁶S. H. Strogatz: Nonlinear dynamics and chaos: with applications

- to physics, biology, chemistry, and engineering (Westview Press, Boulder, 2014).
- ⁷⁷J. K. G. Dhont: An Introduction to Dynamics of Colloids (Elsevier, Amsterdam, 1996).
- $^{78}\mathrm{J}.$ Rotne and S. Prager: J. Chem. Phys $\mathbf{50}$ (1969) 4831.
- ⁷⁹M. J. Lighthill: Comm. Pure Appl. Math. **5** (1952) 109.
- ⁸⁰J. R. Blake: J. Fluid Mech. **46** (1971) 199.
- $^{81}\mathrm{I.}$ O. Götze and G. Gompper: Phys. Rev. E $\mathbf{82}$ (2010) 041921.
- ⁸²M. Theers, E. Westphal, G. Gompper, and R. G. Winkler: Phys. Rev. E **93** (2016) 032604.
- ⁸³J. Blaschke, M. Maurer, K. Menon, A. Zöttl, and H. Stark: Soft Matter 12 (2016) 9821.
- ⁸⁴I. Llopis and I. Pagonabarraga: J. Non-Newtonian Fluid Mech. 165 (2010) 946.
- ⁸⁵R. Singh, S. Ghose, and R. Adhikari: J. Stat. Mech. Theor. Exp. 2015 (2015) P06017.
- $^{86}{\rm G.}$ Nägele: Phys. Rep. ${\bf 272}~(1996)~215.$
- ⁸⁷E. Wajnryb, K. A. Mizerski, P. J. Zuk, and P. Szymczak: J. Fluid Mech. **731** (2013).
- ⁸⁸A. Laskar, R. Singh, S. Ghose, G. Jayaraman, P. B. S. Kumar, and R. Adhikari: Sci. Rep. 3 (2013) 1964.
- ⁸⁹R. K. Manna, P. B. S. Kumar, and R. Adhikari: J. Chem. Phys. 146 (2017) 024901.
- ⁹⁰C. J. Chan, A. E. Ekpenyong, S. Golfier, W. Li, K. J. Chalut, O. Otto, J. Elgeti, J. Guck, and F. Lautenschläger: Biophys. J. 108 (2015) 1856.
- ⁹¹D. Humphrey, C. Duggan, D. Saha, D. Smith, and J. Käs: Nature 416 (2002) 413.
- ⁹²F. Ziebert and I. S. Aranson: Phys. Rev. E **77** (2008) 011918.
- ⁹³I. Bronshtein, E. Kepten, I. Kanter, S. Berezin, M. Lindner, A. B. Redwood, S. Mai, S. Gonzalo, R. Foisner, Y. Shav-Tal, and Y. Garini: Nat. Commun. 6 (2015) 8044.